

Conversion of Xylose into Furfural Catalyzed by Bifunctional Acidic Ionic Liquid Immobilized on the Surface of Magnetic γ - Al_2O_3

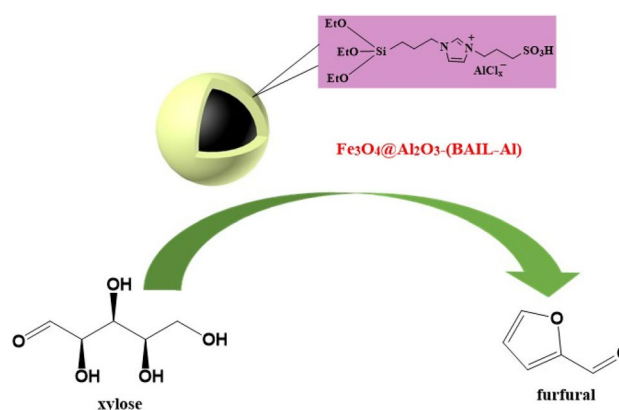
Chunyan Wu¹ · Wenwen Yuan¹ · Yi Huang¹ · Yongmei Xia³ · Huamei Yang² · Haijun Wang¹ · Xiang Liu¹

Received: 6 December 2016 / Accepted: 13 January 2017
© Springer Science+Business Media New York 2017

Abstract A novel heterogeneous catalyst was prepared by immobilizing bifunctional acidic ionic liquid of metal Al substituted (BAIL-Al) onto the surface of magnetic γ - Al_2O_3 , and characterized by FT-IR, TG, XRD, BET, XPS, VSM, SEM and TEM. The catalytic activity of the prepared solid catalyst was investigated for the conversion of xylose to furfural. On the basis, the effects of temperature, time, amount of catalyst and solvent were studied on the yield of furfural. A furfural yield of 67.5% with 97.3% xylose conversion was obtained from xylose using $\text{Fe}_3\text{O}_4@ \text{Al}_2\text{O}_3$ -BAIL-Al as the catalyst in DMSO at 140 °C for 3 h. The immobilized catalyst has the features of easily separation and recycling as well as good thermal stability. Thus, the immobilized catalyst can be efficiently and easily recycled at least five times without apparent loss of activity in xylose conversion and furfural yield.

Graphical Abstract A novel heterogeneous catalyst was prepared by immobilized bifunctional acidic ionic liquid (BAIL-Al) onto the surface of magnetic γ - Al_2O_3 ,

possessing unique physicochemical properties and excellent catalytic activity for xylose transformation have been developed.



Keywords Xylose · Bifunctional acidic ionic liquid (BAIL) · Fe_3O_4 nanoparticles · Magnetic γ - Al_2O_3 · Furfural

Electronic supplementary material The online version of this article (doi:10.1007/s10562-017-1982-z) contains supplementary material, which is available to authorized users.

✉ Huamei Yang
yhmcumt@yeah.net

✉ Haijun Wang
wanghj329@outlook.com

- ¹ The Key Laboratory of Food Colloids and Biotechnology, Ministry of Education, School of Chemical and Material Engineering, Jiangnan University, Wuxi 214122, China
- ² School of Chemistry and Chemical Engineering, Xuzhou University of Technology, Xuzhou 221000, Jiangsu, China
- ³ State Key Laboratory of Food Science & Technology, Wuxi 214122, Jiangsu, China

1 Introduction

With the increasing consumption of fossil fuels and serious pollution of the living environment, to research and development renewable energy has been one of the top priorities for scientists. Biomass is a kind of renewable energy with great prospects. As the main part of biomass, carbohydrate can be used to prepare into a variety of furan derivatives [1, 2]. Furfural is a typical furan derivative with active chemical properties, which can be used to prepare high value-added fine chemicals and liquid fuels [3]. Furfural and its derivatives not only can be used in alkanes to prepare diesel fuel, but also can be used as the basic materials for the

manufactures of gasoline, diesel and aviation kerosene [4, 5]. For instance, furfural can be converted into furan biofuels of 2-methylfuran and 2-methyltetrahydrofuran, wherein 2-methyltetrahydrofuran can be directly used to manufacture gasoline as a basic material [6]. There is no doubt that the demand for furfural in various fields will continue to increase all over the world due to the growing global energy crisis [7].

Many industrial processes of furfural production have been applied, such as Biofine process, CMIV process, Suprayield process, and so on [8]. Studies on methods of better furfural production have never stopped until now. Morais et al. introduced a novel and green approach to produce furfural from xylose and biomass hemicellulose in biphasic system using high-pressure CO₂ as an efficient and sustainable catalyst [9, 10]. Peleteiro et al. reported that furfural was simply and efficiently obtained from eucalyptus wood and xylose using an acidic ionic liquid as a reaction medium and a catalyst [11–13]. As green solvents and catalysts, ionic liquids have been received considerable interest in the conversion of biomass because of unique properties, such as low volatility, high thermal stability, negligible vapor pressure and so on [14–16]. It was reported that high yield of furfural from xylose could be gained in ionic liquids [17]. Furfural was a renewable platform chemical with a bright future and technologies based on ionic liquids were suitable for furfural production [18]. In addition, Yang et al. have shown that furfural can be produced effectively from xylose using AlCl₃·6H₂O as catalyst and NaCl as co-catalyst in THF/H₂O biphasic system [19]. Zhang et al. used AlCl₃ as catalyst in [BMIM]Cl ionic liquid to produce furfural from xylose, and 82.8% furfural yield was obtained at 160 °C [20]. It is believed that ionic liquids combined with aluminum salts have excellent catalytic performance, however, they also exist serious drawbacks of separation and recycling. In order to solve these problems, supported ionic liquids catalysts have been studied, which combine the advantages of homogeneous and heterogeneous catalysts, with the properties of high catalytic performance, easy separation, great reusability, etc. [21].

Over the past several decades, magnetic solid catalysts have been widely applied in the conversion of biomass because of great stability, facile synthesis and easy separation [22]. An efficient catalyst of magnetic material grafted with acidic polyionic liquids was designed and used in the synthesis of promising liquid fuel 5-ethoxymethylfurfural (EMF) from HMF and fructose-based carbohydrates, showing high catalytic activity and stability [23]. A magnetic catalyst of Pb/C@Fe₃O₄ was synthesized by immobilizing Pb on the core-shell structure C@Fe₃O₄ magnetic microspheres, which also showed high activity and extraordinary stability during the oxidation of HMF into 2,5-furandicarboxylic acid (FDCA) under

mild conditions [24]. These magnetic nanoparticles have great stability, and can be easily recovered by an external magnet, which is consistent with the concept of green chemistry.

Efficient production of furfural from xylose could be achieved by using a one-pot combination of xylose-to-xylulose isomerization via Lewis acidic sites and xylulose dehydration via Brønsted acidic sites [19, 25]. Thus, a bifunctional heterogeneous catalyst with Lewis and Brønsted acidic sites should be a better choice to convert xylose into furfural. On the surface of catalyst, Brønsted acid sites (proton donors) can be generated from highly polarized hydroxyl groups. They can also form on oxide-based catalysts via proton balance of a net negative charge introduced by substituting cations with a lower valence charge. Lewis acid sites are formed from coordinative unsaturated cationic sites, which leave Mn⁺ exposed to interact with guest molecules as an acceptor of an electron pair [26]. Mesoporous γ-Al₂O₃ is widely used as a support because of its high specific areas, which provides a greater contact area and possibly a higher number of active site for the desired reactions to occur [27]. At the same time, γ-Al₂O₃ has Lewis acidic sites which are benefit to the conversion of xylose [28]. From our previous work, a bifunctional ionic liquid with high activity is a better choice for the conversion of biomass [29].

In this work, we synthesized a new catalyst with bifunctional ionic liquids immobilized on the surface of magnetic γ-Al₂O₃, which has strong Lewis and Brønsted acidic sites. Furthermore, the catalyst exhibits efficient activity for the dehydration of xylose into furfural.

2 Experimental Section

2.1 Materials

FeCl₃·6H₂O, FeSO₄·7H₂O, Al(NO₃)₃·9H₂O, NH₄HCO₃, ammonium hydroxide (28 wt%), Cetyltrimethylammonium bromide (CTAB), Imidazole and Sodium ethoxide were purchased from Sinopharm Chemical Reagent Co. Ltd. (Shanghai, China). γ-Chloropropyl Triethoxysilane (CPTES) and 1,3-Propanesultone were purchased from Aladdin Industrial Inc. (Shanghai, China). Furfural and xylose were also obtained from Sinopharm Chemical Reagent Co. Ltd. (Shanghai, China). All solvents and reagents were purchased from commercial sources and were used without further purification. Deionized water was produced with a laboratory water-purification system (RO DI Digital plus).

2.2 Synthesis of the Bifunctional Acidic Ionic Liquid Supported on Magnetic γ -Al₂O₃ Material

2.2.1 Synthesis of γ -Al₂O₃ Nanoparticles

γ -Al₂O₃ was prepared using sol-gel method. At first, 1 g L⁻¹ CTAB solution was prepared with distilled water. Then, Al(NO₃)₃·9H₂O and NH₄HCO₃ were respectively dissolved in the above solution in order to have the mixture solution concentration of 27 and 12%. NH₄HCO₃ solution was slowly added to Al(NO₃)₃ solution under vigorously stirring. NH₄HCO₃ solution was stopped dropping until the sol was completely formed which was continued to stir for 1 h and age for 48 h. The prepared sol was filtered and dried in vacuum at 60 °C for 6 h. Finally, the xerogel powder was calcined at 550 °C for 3 h, and γ -Al₂O₃ nanoparticles were obtained.

2.2.2 Synthesis of the Bifunctional Acidic Ionic Liquids

The bifunctional acidic ionic liquids were prepared according to the literature method with a modification [30]. Imidazole (3.4 g) and CPTES (12 g) were dissolved in toluene and refluxed for 24 h at 110 °C under N₂ atmosphere. After reaction, 1,3-Propanesultone (6.1 g) was added to the above mixture solution and stirred for 24 h continuously. The solvent was evaporated under reduced pressure and the obtained product was washed three times with diethyl ether. The obtained compound was dissolved in ethanol and HCl was slowly added to the solution at 70 °C for 2 h. Then, metal chlorides were added to the above mixture solution and stirred for another 2 h. The mixture was filtered and evaporated under reduced pressure. The obtained product was vacuum-dried at 40 °C for 12 h. Finally, the target bifunctional acidic ionic liquids (BAIL-M) were obtained. The acid ionic liquid (AIL-Cl) and bifunctional acid ionic liquids (BAIL-Al, BAIL-Cr, BAIL-Sn, BAIL-Fe) were characterized by FT-IR (see supporting information Fig. S1).

2.2.3 Synthesis of the Bifunctional Ionic Liquid Supported on γ -Al₂O₃ Material

Typically, γ -Al₂O₃ (1 g) and (BAIL-Al) (2 g) were added to 50 mL mixture solution of dry toluene under stirring. The suspension was refluxed for 24 h under nitrogen atmosphere. After reaction, the resulting mixture was cooled and filtered under reduced pressure. The obtained material was washed three times with ethanol and dried in the oven at 40 °C overnight. The obtained material was denoted as γ -Al₂O₃-(BAIL-Al).

2.2.4 Synthesis of Fe₃O₄ Nanoparticles

The Fe₃O₄ nanoparticles were prepared through a coprecipitation method [31]. Firstly, FeCl₃·6H₂O (6.76 g) and FeSO₄·7H₂O (3.8 g) were added to 100 mL of deionized water under vigorous stirring. Secondly, ammonium hydroxide (28 wt%) was added to the solution until pH 10 was reached. Thirdly, the mixture solution was stirred for 2 h under the condition of 60 °C. Finally, the precipitates were collected with magnet and were washed three times with deionized water and ethanol successively. After that, the magnetic NPs were dried in an oven at 40 °C for 6 h.

2.2.5 Synthesis of the Magnetic Catalyst Material (Fe₃O₄@Al₂O₃-(BAIL-Al))

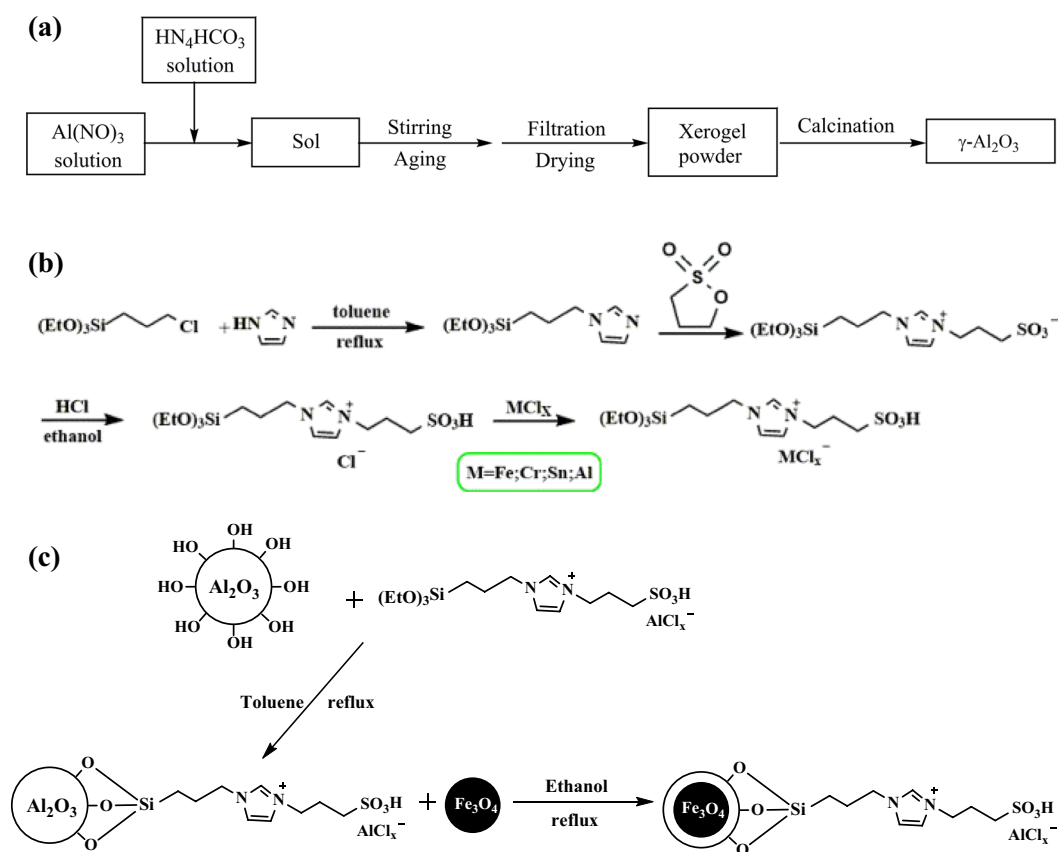
Typically, γ -Al₂O₃-(BAIL-Al) (100 mg) and Fe₃O₄ (20 mg) was added to 20 mL ethanol solution and vigorously stirred for 12 h. After reaction, the catalyst material was separated by magnet, which was dried in the oven at 40 °C overnight. The obtained catalyst was denoted as Fe₃O₄@Al₂O₃-(BAIL-Al), and the synthetic route of the magnetic catalyst was illustrated in Scheme 1.

2.3 Catalyst Characterization

SEM images were obtained via a HITACHI S-4800 field-emission scanning electron microscope. Transmission electron microscopy (TEM) was performed on a JEOL JEM model 2100 microscope operated at 200 kV. FT-IR measurements were recorded on a Nicolet 360 FT-IR instrument (KBr discs) in the wavenumber range of 4000–500 cm⁻¹. Thermogravimetric analysis (TGA) was performed on a STA409 instrument under a nitrogen atmosphere at a heating rate of 20 °C min⁻¹ from 25 to 700 °C. Powder X-ray diffraction (XRD) patterns were collected by using a Bruker D8 Advance powder diffractometer (Cu/K α) in the 2 θ range of 10–80° with a scanning speed of 4°/min at 40 kV and 20 mA. The X-ray photoelectron spectroscopy (XPS) spectra were recorded by Perkin Elmer PHI 5000 ESCT System. The pore volume, pore size and specific surface area were measured by N₂ adsorption/desorption analysis (Micromeritics ASAP 2020) at 77 K using Brunauer–Emmett–Teller (BET) and Barrett–Joyner–Halenda (BJH) methods. Magnetic measurements were carried out using a superconducting quantum interface device magnetometer (SQUID VSM) at room temperature in an applied magnetic field sweeping from –10 kOe to 10 kOe.

2.4 Catalytic Reactions

Typically, a 25 mL Single-necked flask was charged with xylose (100 mg), Fe₃O₄@Al₂O₃-(BAIL-Al) (40 mg) and



Scheme 1 **a** Synthetic route of γ - Al_2O_3 , **b** Synthetic route of bifunctional acidic ionic liquids (BAIL-M), **c** Synthetic route of BAIL-Al immobilized on magnetic γ - Al_2O_3

DMSO (3 mL). The reaction mixture was performed with vigorous stirring in an oil bath at 140°C for 3 h. After reaction, the reaction mixture was cooled to room temperature, and the catalyst was separated via a magnet. The 50 μL sample was obtained from reaction solution which was diluted with deionized water and analyzed by high-performance liquid chromatography (HPLC).

2.5 Analysis

Liquid samples were analyzed by HPLC using an Agilent 1100 equipped with a refractive index detector, and a Shodex SURGER SP0810 (300 \times 8.0) column at a column temperature of 70°C for analysis. Ultra-pure water was used as the eluent phase with a flow rate of 0.7 mL min^{-1} . The amount of furfural and xylose were determined with an external standard. The conversion of xylose and the yield of furfural were evaluated using the following equations:

$$\text{Xylose conversion (mol\%)} = \left(1 - \frac{\text{moles of remaining xylose}}{\text{moles of starting xylose}} \right) \times 100\%$$

$$\text{Furfural yield (mol\%)} = \left(\frac{\text{moles of furfural}}{\text{moles of starting xylose}} \right) \times 100\%$$

3 Results and Discussion

3.1 Catalyst Characterization

3.1.1 SEM and TEM Analysis

In order to examine the surface morphology and internal composition of nanoparticles, SEM and TEM were conducted. Typical surface SEM images of γ - Al_2O_3 and γ - Al_2O_3 -(BAIL-Al) particles are illustrated in Fig. 1a, b, respectively. It can be observed that the morphology of γ - Al_2O_3 has been changed drastically as its surface has been covered chemically with acidic ionic liquid [32]. The core-shell structure of magnetic catalyst was conducted by TEM characterization as shown in Fig. 1c, d. The apparent dark area was the nuclear center of Fe_3O_4 , which was surrounded by a grey layer of the coated

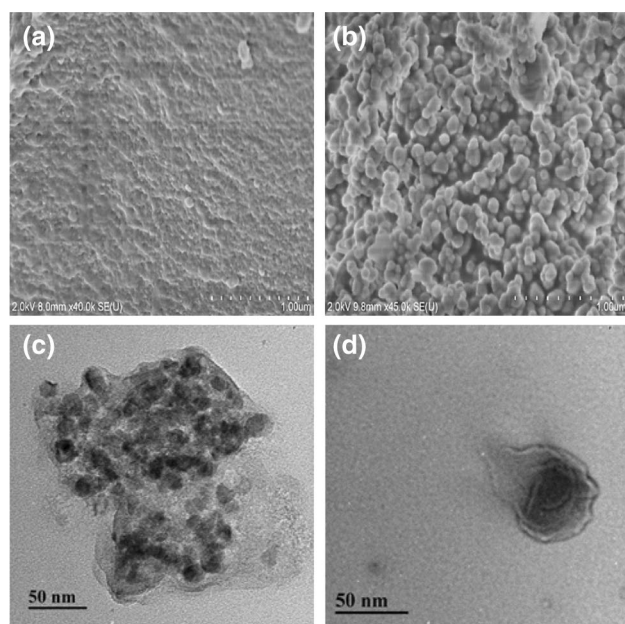


Fig. 1 SEM images of **a** γ - Al_2O_3 and **b** γ - Al_2O_3 -(BAIL-Al) nanoparticles, TEM image of the catalyst **(c)** and **(d)** Fe_3O_4 @ Al_2O_3 -(BAIL-Al)

material, and the average size of the obtained particles was 40–50 nm [33].

3.1.2 FT-IR Spectroscopy

The structure of the Fe_3O_4 @ Al_2O_3 -(BAIL-Al) catalyst was characterized by FT-IR technology, the resulting image shown in Fig. 2. The typical band at 569 cm^{-1} was the characteristic Fe–O vibration of Fe_3O_4 , and the peak at 638 cm^{-1} was the Al–O vibration of Al_2O_3 . The FT-IR spectra displayed the peak at 1045 cm^{-1} , belonging to the Si–O stretching vibration. The broad peak at 3426 cm^{-1} was attributed to the stretching vibration of O–H in carrier and absorbed water. The peak at 1641 cm^{-1} was related to OH bending vibration in the surface of carrier [34]. At the same time, two characteristic peaks at 1568 and 1458 cm^{-1} were the C=C and C=N stretching vibration of the imidazole ring [29]. In addition, the 2931 cm^{-1} band was attributed to the stretching vibration of alkyl chain. The presence of $-\text{SO}_3\text{H}$ group was verified by S=O stretching vibration appearing at 1139 cm^{-1} [35]. These results indicated the acidic ionic liquid was supported on the magnetic γ - Al_2O_3 successfully.

3.1.3 Thermal Analysis

TGA curves of Fe_3O_4 , γ - Al_2O_3 -(BAIL-Al) and the catalyst Fe_3O_4 @ Al_2O_3 -(BAIL-Al) were shown in Fig. 3,

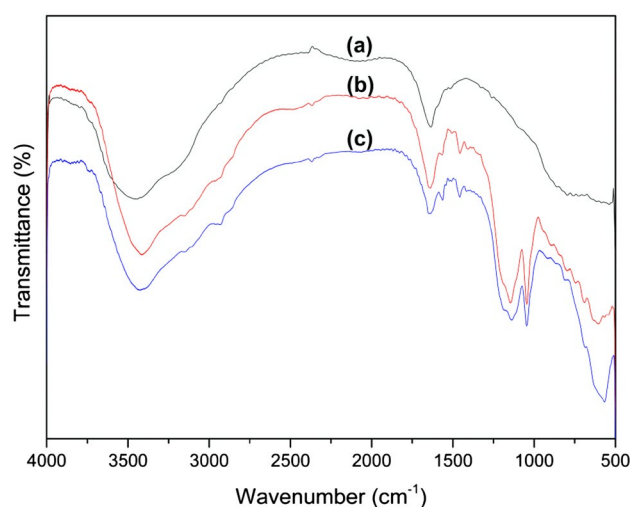


Fig. 2 FT-IR spectrums of **a** γ - Al_2O_3 , **b** γ - Al_2O_3 -(BAIL-Al) and **c** Fe_3O_4 @ Al_2O_3 -(BAIL-Al)

which were used to investigate the stability of the catalyst. For the catalyst Fe_3O_4 @ Al_2O_3 -(BAIL-Al), a small amount of weight loss of the catalyst in the range of 50–100 °C was due to the removal of physically adsorbed water on the surface of the mesoporous material. Meanwhile, the minor wrapped water of the porosity of mesoporous particles was eliminated between 100 and 300 °C. Furthermore, in the range of 300–500 °C, thermal decomposition of the bifunctional acidic ionic liquid resulted in the fasted weight loss of the catalyst and rapid decline of TG curve with increasing temperature. It was demonstrated that the catalyst exhibited good thermal stability below 300 °C.

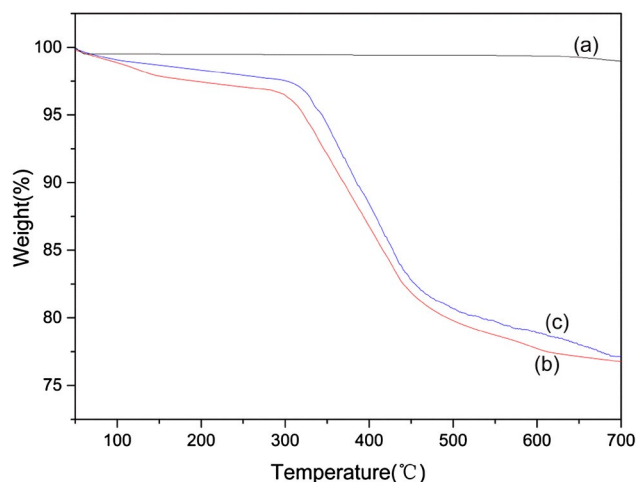


Fig. 3 TGA curves of **a** Fe_3O_4 , **b** γ - Al_2O_3 -(BAIL-Al) and the catalyst **c** Fe_3O_4 @ Al_2O_3 -(BAIL-Al)

3.1.4 Wide Angle X-ray Diffraction Study

The XRD patterns of Fe_3O_4 and $\text{Fe}_3\text{O}_4@ \text{Al}_2\text{O}_3\text{-}(\text{BAIL-Al})$ were shown in Fig. 4. The pattern of the catalyst showed the presence of characteristic diffraction peaks at $2\theta = 30.3^\circ$, 35.4° , 43.2° , 53.7° , 57.1° and 63.0° . These peaks were assigned to the (220), (311), (400), (422), (511) and (440) crystal plane diffraction peaks of Fe_3O_4 [36]. The pattern showed the diffraction peaks at $2\theta = 37.0^\circ$, 46.3° and 66.9° were the characteristic peaks of $\gamma\text{-Al}_2\text{O}_3$ [37]. The same peaks of XRD patterns were observed in both of the Fe_3O_4 and $\text{Fe}_3\text{O}_4@ \text{Al}_2\text{O}_3\text{-}(\text{BAIL-Al})$, indicating that the nanoparticle was pure Fe_3O_4 with a spinel structure and that the wrapped process did not induce any phase change of Fe_3O_4 [38]. At the same time, the XRD patterns of $\gamma\text{-Al}_2\text{O}_3$ and $\gamma\text{-Al}_2\text{O}_3\text{-}(\text{BAIL-Al})$ were compared (see supporting information Fig. S2).

3.1.5 X-ray Photoelectron Spectroscopy (XPS) Analysis

The XPS image of the surface element composition of $\text{Fe}_3\text{O}_4@ \text{Al}_2\text{O}_3\text{-}[\text{BAIL-Al}]$ catalyst was shown in Fig. 5. The peaks with binding energy at 531.8, 399.3, 285.6, 198.7, 168.4, 151.5, 118.2, 100.3 and 73.6 eV were corresponded to O1s, N1s, C1s, Cl S, Si2s, Al2s, Si2p and Al2p, respectively. These XPS results indicated that the bifunctional acidic ionic liquid was immobilized on $\gamma\text{-Al}_2\text{O}_3$ successfully due to the existence of N, C, S, Cl and Si in the surface of the catalyst. The XPS results also showed that there were no iron present on the surface of the catalyst, indicating that Fe_3O_4 was encapsulated by a layer, consistent with the TEM results as shown in Fig. 1,

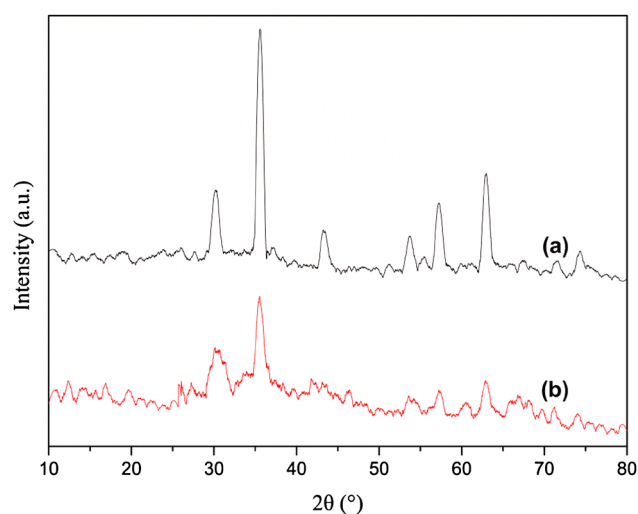


Fig. 4 Wide angle powder XRD patterns of *a* Fe_3O_4 and *b* $\text{Fe}_3\text{O}_4@ \text{Al}_2\text{O}_3\text{-}(\text{BAIL-Al})$

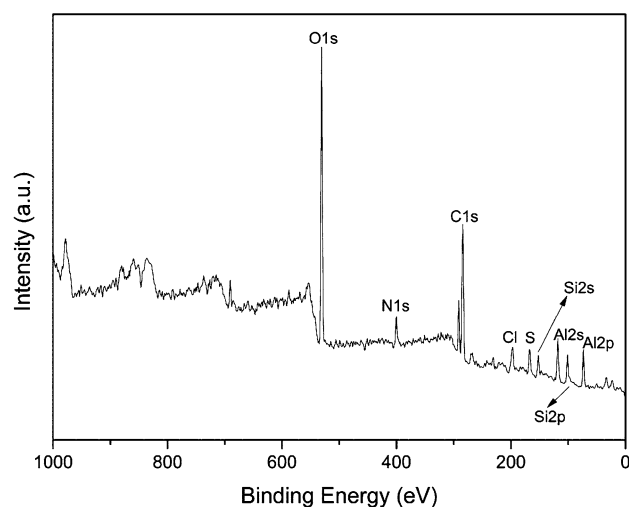


Fig. 5 XPS spectrum of the $\text{Fe}_3\text{O}_4@ \text{Al}_2\text{O}_3\text{-}(\text{BAIL-Al})$ catalyst

in which a thin $\gamma\text{-Al}_2\text{O}_3\text{-}[\text{BAIL-Al}]$ layer was observed [23].

3.1.6 N_2 Sorption Studies

The nitrogen adsorption–desorption isotherms and pore size distributions of $\gamma\text{-Al}_2\text{O}_3$ and $\text{Al}_2\text{O}_3\text{-}(\text{BAIL-Al})$ samples, as shown in Fig. 6. According to the International Union of Pure and Applied Chemistry (IUPAC) classification, both materials have a type-IV-shaped isotherm and a mesoporous structure (pore diameter between 2 and 50 nm) [39]. The surface area, pore size distribution and average pore diameter were displayed in Table 1. The results showed that the surface modification over bifunctional acidic ionic liquid has substantially maintained the

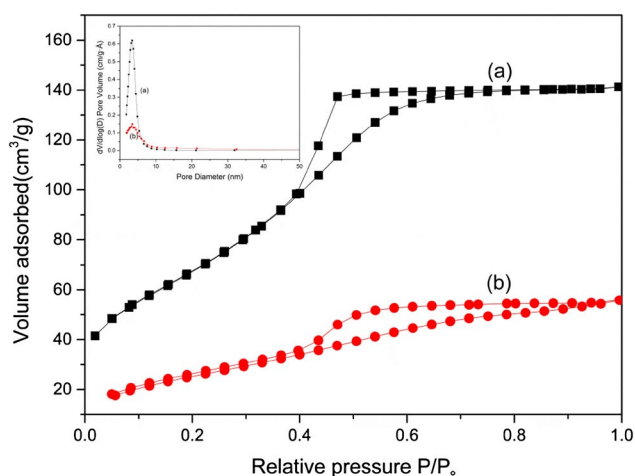


Fig. 6 Nitrogen physisorption isotherms and pore size distribution for the *a* $\gamma\text{-Al}_2\text{O}_3$, *b* $\gamma\text{-Al}_2\text{O}_3\text{-}(\text{BAIL-Al})$

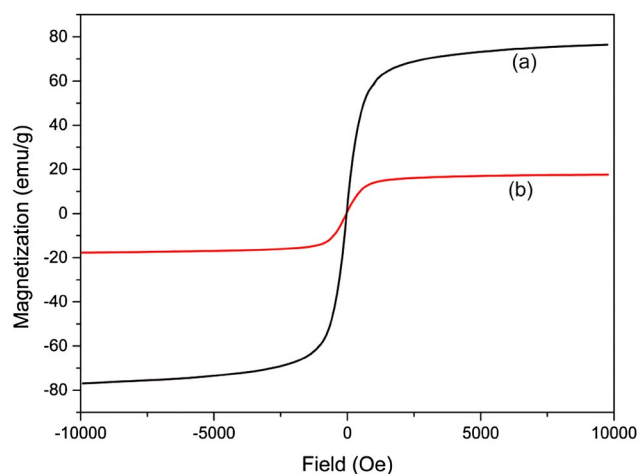
Table 1 Physical properties of $\gamma\text{-Al}_2\text{O}_3$ and $\gamma\text{-Al}_2\text{O}_3\text{-(BAIL-Al)}$

Entry	Sample type	Surface area ($\text{m}^2 \text{g}^{-1}$)	Pore volume ($\text{cm}^3 \text{g}^{-1}$)	Average pore diameter (nm)
1	$\gamma\text{-Al}_2\text{O}_3$	247.0	0.22	3.54
2	$\gamma\text{-Al}_2\text{O}_3\text{-(BAIL-Al)}$	94.3	0.09	3.66

mesoporous structure. A decrease in surface area was observed for $\gamma\text{-Al}_2\text{O}_3$ and $\text{Al}_2\text{O}_3\text{-(BAIL-Al)}$ from 247.0 to 94.3 $\text{m}^2 \text{g}^{-1}$ and the pore volume decreased from 0.22 to 0.09 $\text{cm}^3 \text{g}^{-1}$, but the average pore diameters increased from 35 to 37 Å, which suggested that bifunctional acidic ionic liquid may be well confined in the surface of mesoporous $\gamma\text{-Al}_2\text{O}_3$. In addition, the pore volume, pore size and specific surface area of the catalyst $\text{Fe}_3\text{O}_4@ \text{Al}_2\text{O}_3\text{-(BAIL-Al)}$ was exhibited (see supporting information Table S1 and Fig S3).

3.1.7 Magnetic Analysis

The magnetization curves of the carrier and catalyst were measured by a vibrating sample magnetometer (VSM) at room temperature (298 K), as shown in Fig. 7. Saturation magnetization of the Fe_3O_4 was 76.4 emu g^{-1} and saturation magnetization of the catalyst was 17.5 emu g^{-1} . The saturation magnetization of the immobilized material decreased due to the introduction of acidic ionic liquid, weakening the saturation magnetization. Moreover, the room temperature magnetization curves of the carrier and immobilized catalyst exhibited no hysteresis which demonstrated their superparamagnetic characteristics [40].

**Fig. 7** The magnetization curves of the Fe_3O_4 (a) and the catalyst $\text{Fe}_3\text{O}_4@ \text{Al}_2\text{O}_3\text{-(BAIL-Al)}$ (b)

The results of VSM showed that the prepared catalyst still had good magnetic property. Therefore, the catalyst could be separated magnetically from the mixing system at the end of the reaction.

3.2 Conversion of Xylose to Furfural by the Acidic Ionic Liquids

The effects of different metal substituted acidic ionic liquids on the transformation of xylose to furfural were investigated in DMSO and the results were listed in Table 2. The acidic ionic liquid (AIL-Cl) had a little catalytic activity for the dehydration of xylose at 140 °C for 1 h, a furfural yield of 33% was obtained (Table 2, entry 1). Bifunctional acidic ionic liquids of different metal substituted had better catalytic activity, and the bifunctional acidic ionic liquid of Al substituted (BAIL-Al) was the best among them. A furfural yield of 73.5% with 93.7% xylose conversion was achieved by BAIL-Al (Table 2, entry 5). It is superior to some other ionic liquids because high furfural yield could be obtained using BAIL-Al with shorter time [12]. So it is indicated that BAIL-Al has the best catalytic activity, which is benefit to convert xylose to furfural.

3.3 Conversion of Xylose to Furfural by the Immobilized Catalyst

Based on the above researches, the bifunctional acidic ionic liquid (BAIL) showed the best catalytic activity on the conversion of xylose to furfural. Therefore, the dehydration of xylose to furfural was measured using the immobilized catalyst $\text{Fe}_3\text{O}_4@ \text{Al}_2\text{O}_3\text{-(BAIL-Al)}$. Furthermore, influences of solvent, temperature, time and amount of catalyst were studied on the conversion of xylose to furfural.

3.3.1 Effect of Solvent

During the reaction process of dehydration of xylose to furfural using the catalyst $\text{Fe}_3\text{O}_4@ \text{Al}_2\text{O}_3\text{-(BAIL-Al)}$, the solvent effect was very obvious. The result was consistent

Table 2 The catalytic activity of different metal substituted acidic ionic liquids on the conversion of xylose to furfural

Entry	Catalyst	Xylose conversion (%)	Furfural yield (%)
1	AIL-Cl	61.3	33.0
2	BAIL-Fe	75.4	40.3
3	BAIL-Cr	83.3	48.2
4	BAIL-Sn	89.5	63.4
5	BAIL-Al	93.7	73.5

Reaction conditions: 100 mg of xylose, 3 mL of DMSO, 20 mg catalyst, T = 140 °C, t = 1 h

Table 3 The effect of different solvents on the conversion of xylose to furfural

Entry	Solvent	Xylose conversion (%)	Furfural yield (%)
1	DMSO	97.3	67.5
2	DMF	73.4	40.2
3	DMA	70.2	38.6
4	NMP	69.3	37.3
5	Toluene	88.4	51.9
6	n-Butanol	90.6	55.8
7	Ethanol	86.5	16.7
8	DMSO-H ₂ O ^a	75.1	44.5

Reaction conditions: 100 mg of xylose, 3 mL of solvent, 40 mg of catalyst, T = 140 °C, t = 3 h

^aVolume ratio of H₂O/DMSO = 1:5

with the research that the furfural yield was changed obviously while different solvents were incorporated to the reaction media [13, 41]. Therefore, we inspected the impact of different solvents on the furfural yield using the catalyst Fe₃O₄@Al₂O₃-(BAIL-Al), such as Dimethyl sulfoxide (DMSO), *N,N*-Dimethylformamide (DMF), *N,N*-Dimethylacetamide (DMA), 1-Methyl-2-pyrrolidone (NMP), toluene, n-butanol and ethanol, as shown in Table 3.

From the above table, we could find that the catalyst Fe₃O₄@Al₂O₃-(BAIL-Al) showed the best catalytic activity when DMSO as the reaction solvent under the same reaction conditions, it was corresponded to the study of Li and co-workers [42]. Most of xylose was transformed, and 67.5% furfural yield was obtained. The result was consistent with the study that DMSO could improve selectivity and dehydration rate in formation of furfural [43]. Obviously, n-butanol, toluene, DMF, DMA and NMP were relatively less efficient solvents in this reaction, with furfural yield of 55.8%, 51.9%, 40.2%, 38.6% and 37.3%, respectively. In addition, the lowest catalytic activity was showed in furfural yield when ethanol as a solvent, which was consistent with the report of Iglesias [44]. The catalytic activity of Fe₃O₄@Al₂O₃-(BAIL-Al) was inhibited significantly when water was added to the reaction. Only 75.1% xylose conversion was obtained at 140 °C for 3 h. Moreover, furfural selectivity was relatively low due to the presence of water which made the reaction equilibrium toward the direction of xylose. At the same time, part of furfural was continued to generate the oxidation or polymerization.

3.3.2 Effect of Reaction Temperature and Time

During the reaction progress of preparation of furfural from xylose, reaction temperature and time were very

important factors. Therefore, we investigated the influence of temperature and time for conversion of xylose to furfural, and the results were shown in Fig. 8. The reaction time was 1–5 h at different temperature ranged from 120 to 150 °C. At 120 °C low temperature phase, xylose degradation rate was relatively slow which caused only 46.9% furfural yield for 5 h in DMSO, because an intermediate product of dehydration was formed at the degradation progress of xylose which did not dehydrate to furfural in time due to low reaction rate. The yield of furfural gradually increased with the growth temperature, and 67.5% furfural yield was obtained at 140 °C for 3 h. The furfural yield was in a similar range to the reported for xylose dehydration using high-pressure CO₂ as a catalyst [10]. While the yield of furfural declined at 150 °C high temperature phase, because the probability of collisions between the reaction molecules was enhanced with the growth temperature, resulting in an increase in the side reaction rate, thereby generating polymers or dehydrated byproducts [45]. Therefore, 140 °C and 3 h were selected as the best reaction temperature and time for the dehydration of xylose to furfural.

3.3.3 Effect of the Amount of Catalyst

Influence of the amount of catalyst on conversion of xylose to furfural was investigated at 140 °C for 3 h in order to optimize the catalytic activity of catalyst Fe₃O₄@Al₂O₃-(BAIL-Al). The effect of varying amounts of catalyst for xylose conversion and furfural yield was shown in Fig. 9. As it can be seen from the figure, when a small amount of catalyst (20 mg) was added, the conversion of

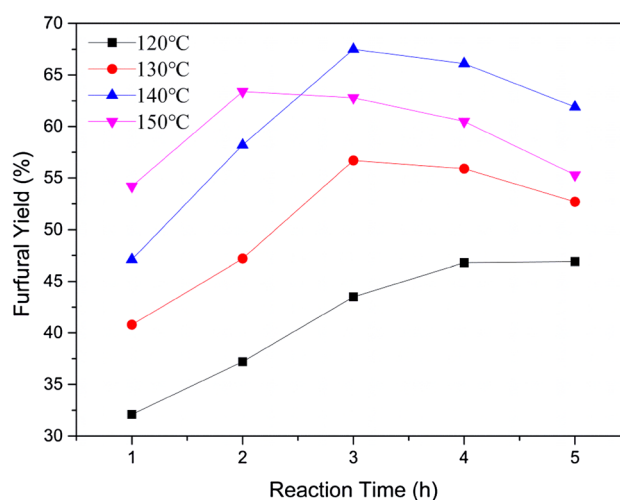


Fig. 8 Influence of reaction temperature and time on the conversion of xylose to furfural. Reaction conditions: 100 mg of xylose, 3 mL of DMSO, 40 mg of catalyst

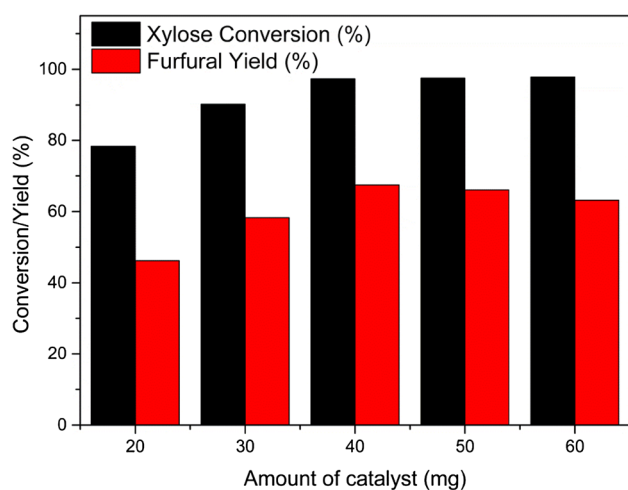


Fig. 9 Effect of the amount of catalyst on xylose conversion and furfural yield. Reaction conditions: 100 mg of xylose, 3 mL of DMSO, $T = 140^{\circ}\text{C}$, $t = 3$ h

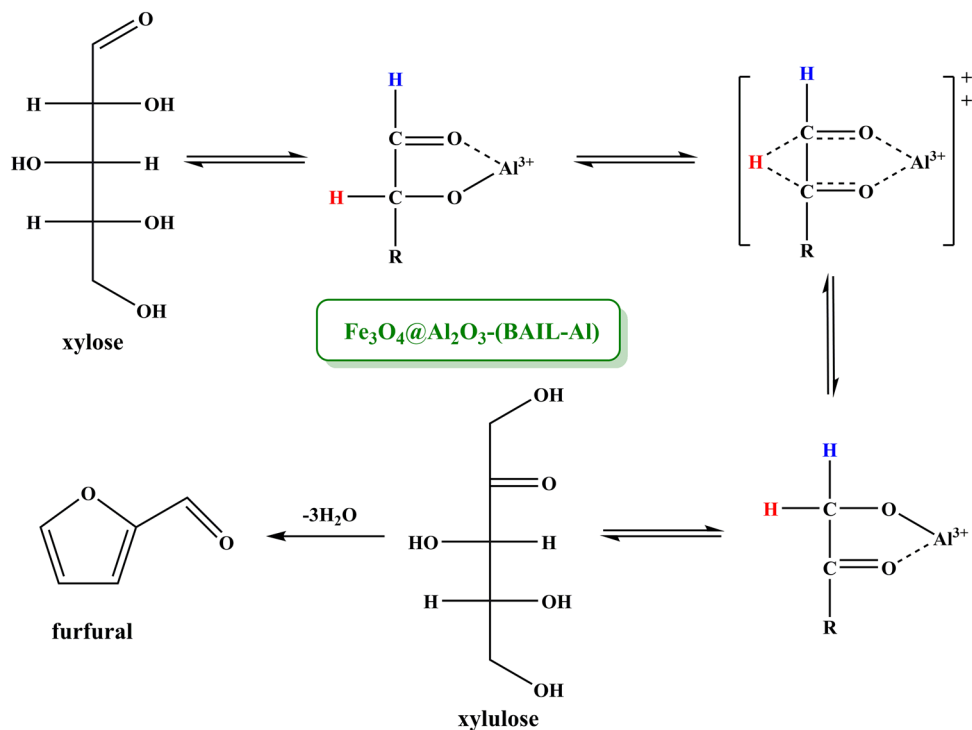
xylose and the yield of furfural reached 78.3% and 46.2% respectively. Further increasing the amount of catalyst, the catalyst activity has been significantly improved. When the amount of catalyst was 40 mg, 97.3% xylose conversion and 67.5% furfural yield were obtained. When the amount of catalyst was continued to increase, the active site of the catalytic reaction was also increased. However, the yield of furfural showed a downward trend under the same reaction conditions, mainly because more

active sites not only promoted a positive reaction, but also accelerated the degradation of furfural or polymerization reaction rate, which led to a decline furfural yield. The results parallel those reported in the literature for the reactions of xylose using ionic liquids [46]. In summary, 40 mg was the optimum amount of catalyst. Based on a large number of references, the plausible reaction mechanism for xylose conversion to furfural was put forward, as shown in Scheme 2 [47–50].

3.3.4 Reusability of the Catalyst

The catalyst $\text{Fe}_3\text{O}_4@ \text{Al}_2\text{O}_3\text{-(BAIL-Al)}$ was reacquired from the mixture by magnetic separation, washed with ethanol and dried at 40°C in an oven. The reaction temperature and time were 140°C and 3 h, respectively. The catalyst was successfully recycled five times for the conversion of xylose to furfural with a slight decrease on catalytic activity, as shown in Fig. 10. The catalyst used for the first time, 67.5% furfural yield was obtained from xylose dehydration. When the catalyst was used at the second time, the catalytic activity was lower slightly, and the yield of furfural was 63.2%. While the catalyst was recycled 5 times, 58.7% furfural yield was obtained. After using repeatedly, the yield of furfural occurred to decrease, because the byproduct of reaction was adhered to the active sites of the catalyst surface, so that the catalyst could not be sufficiently in contact with the substrate during the next course of the reaction, thereby the catalytic result of the reaction was decreased.

Scheme 2 Plausible reaction mechanism for xylose conversion to furfural using $\text{Fe}_3\text{O}_4@ \text{Al}_2\text{O}_3\text{-(BAIL-Al)}$ catalyst



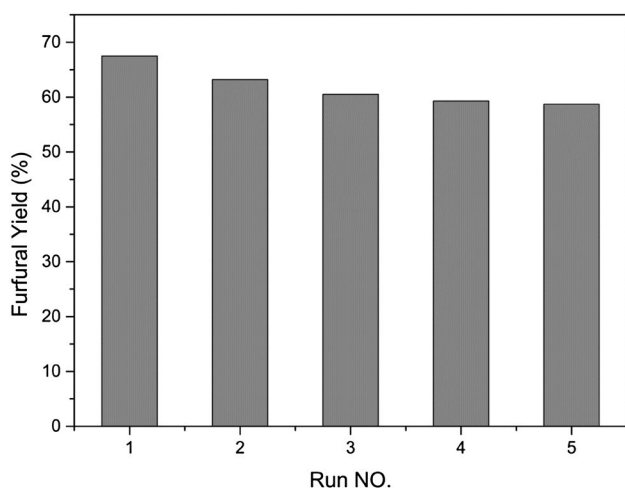


Fig. 10 Reusability of the catalyst on the conversion of xylose into furfural. Reaction conditions: 100 mg of xylose, 40 mg of catalyst, 3 mL of DMSO, $T = 140^{\circ}\text{C}$, $t = 3$ h

In conclusion, reusability of the catalyst $\text{Fe}_3\text{O}_4@ \text{Al}_2\text{O}_3$ - (BAIL-Al) was very well.

4 Conclusion

A series of bifunctional acidic ionic liquids were tested as catalysts for the conversion of xylose to furfural in order to choose the best catalytic activity. The magnetic $\gamma\text{-Al}_2\text{O}_3$ carrier not only has Lewis acidic site, and also has the advantages of readily separation and recycling. A novel heterogeneous catalyst $\text{Fe}_3\text{O}_4@ \text{Al}_2\text{O}_3$ - (BAIL-Al) was synthesized by immobilized bifunctional acidic ionic liquid onto the surface of magnetic $\gamma\text{-Al}_2\text{O}_3$, which was demonstrated to be the most active. A furfural yield of 67.5% with 97.3% xylose conversion was achieved at 140°C for 3 h in DMSO. The immobilized catalyst has been efficiently and easily recycled at least five times without apparent loss of activity in xylose conversion and furfural yield. So it is indicated that the novel heterogeneous catalyst has great potential in industry applications due to its green preparation, high activity and high reusability.

References

- Zhou P, Zhang Z (2016) *Catal Sci Technol* 6(11):3694–3712
- Liu B, Zhang Z (2016) *ChemSusChem* 9(16):2015–2036
- Bozell JJ, Petersen GR (2010) *ChemInform* 12(28):539–554
- Corma A, de la Torre O, Renz M, Vollandier N (2011) *Angew Chem Int Ed* 50(10):2375–2378
- Corma A, de la Torre O, Renz M (2011) *ChemSusChem* 4(11):1574–1577
- Chheda JN, Románleshkov Y, Dumesic JA (2007) *Green Chem* 9(4):342–350
- Dias AS, Lima S, Pillinger M, Valente AA (2006) *Carbohydr Res* 341(18):2946–2953
- Jong WD, Marcotullio G (2010) *Int J Chem React Eng* 8(1):47–54
- Morais ARC, Matuchaki MDDJ, Andreus J, Bogel-Lukasik R (2016) *Green Chem* 18(10):2985–2994
- Morais ARC, Bogellukasik R (2016) *Green Chem* 18(8):2331–2334
- Peleteiro S, Santos V, Garrote G, Parajó JC (2016) *Carbohydr Polym* 146:20–25
- Peleteiro S, Santos V, Parajó JC (2016) *Carbohydr Polym* 153:421–428
- Peleteiro S, Lopes AMDC, Garrote G, Parajó JC, Bogel-Lukasik R (2015) *Ind Eng Chem Res* 54:8368–8373
- Zhang Z, Zhao ZK (2010) *Bioresour Technol* 101(3):1111–1114
- Liu B, Zhang Z, Zhao ZK (2013) *Chem Eng J* 215–216(3):517–521
- Xiong Y, Zhang Z, Wang X, Liu B, Lin J (2014) *Chem Eng J* 235 (1):349–355
- Matsagar BM, Munshi MK, Kelkar AA, Dhepe PL (2015) *Catal Sci Technol* 5(12):5086–5090
- Peleteiro S, Rivas S, Alonso JL, Santos V, Parajó JC (2016) *Bioresour Technol* 202:181–191
- Yang Y, Hu CW, Abu-Omar MM (2012) *ChemSusChem* 5(2):405–410
- Zhang L, Yu H, Pan W, Dong H, Peng X (2012) *Bioresour Technol* 130C(2):110–116
- Wu Z, Li Z, Wu G, Wang L, Lu S, Wang L, Wan H, Guan G (2014) *Ind Eng Chem Res* 53(8):3040–3046
- Liu B, Zhang Z (2016) *ACS Catal* 6(1):326–338
- Yin S, Sun J, Liu B, Zhang Z (2015) *J Mater Chem A* 3(9):4992–4999
- Liu B, Ren Y, Zhang Z (2014) *Green Chem* 17 (3):1610–1617
- Agirrezabal-Telleria I, García-Sancho C, Maireles-Torres P, Arias PL (2013) *Chin J Catal* 34(7):1402–1406
- Weingarten R, Tompsett GA, Conner WC, Huber GW (2011) *J Catal* 279(279):174–182
- Thyssen VV, Maia TA, Assaf EM (2015) *J Braz Chem Soc* 26 (1):22–31
- Jeness GR, Christiansen MA, Caratzoulas S, Vlachos DG, Gorte RJ (2014) *J Phys Chem C* 118(24):12899–12907
- Wang Y, Gu Z, Liu W, Yao Y, Wang H, Xia XF, Li W (2015) *RSC Adv* 5(75):60736–60744
- Safaei S, Mohammadpoorbaltork I, Khosropour AR, Moghadam M, Tangestaninejad S, Mirkhani V (2013) *Catal Sci Technol* 3(10):2717–2722
- Jing H, Wang X, Liu Y, Wang A (2015) *Chin J Catal* 36 (2):244–251
- Taghavi M, Ghaemy M, Nasab SMA, Hassanzadeh M (2015) *J Polym Res* 22(2):1–12
- Gu Z, Wang Y, Yao Y, Xia X, Wang H, Li W (2015) *Catal Lett* 145(12):2046–2054
- Habibi N, Arandiyani H, Rezaei M (2016) *RSC Adv* 6(35):29576–29585
- Zhang Q, Luo J, Wei Y (2011) *ChemInform* 42(14):2246–2254
- Zheng J, Dong Y, Wang W, Ma Y, Hu J, Chen X, Chen X (2013) *Nanoscale* 5(11):4894–4901
- Yaripour F, Shariatnia Z, Sahebdehfar S, Irandoukht A (2015) *Fuel* 139(139):40–50
- Azgoni M, Mokhtary M (2015) *J Mol Catal A* 398 (4):58–64
- Masouleh NSG, Taghizadeh M, Yaripour F (2014) *Chem Eng Technol* 37(9):1475–1482
- Zhang Q, Su H, Luo J, Wei Y (2012) *ChemInform* 14(25):201–208

41. Peleteiro S, Lopes AMDC, Garrote G, Bogel-Lukasik R, Parajó JC (2015) *Ind Crops Prod* 77:163–166
42. Hu X, Westerhof R, Dong D, Wu L, Li CZ (2014) *ACS Sustain Chem Eng* 2(11):2562–2575
43. Rong C, Ding X, Zhu Y, Li Y, Wang L, Qu Y, Ma X, Wang Z (2012) *Carbohydr Res* 350(350):77–80
44. Iglesias J, Melero JA, Morales G, Paniagua M, Hernández B (2016) *ChemCatChem* 8(12):2089–2099
45. Huang R, Qi W, Su R, He Z (2010) *ChemInform* 46(24):1115–1117
46. Lima S, Neves P, Antunes MM, Pillinger M, Ignatyev N, Valente AA (2009) *Appl Catal A* 363(1–2):93–99
47. Zhang Z, Du B, Quan ZJ, Da YX, Wang XC (2014) *Catal Sci Technol* 4(3):633–638
48. Choudhary V, Sandler SI, Vlachos DG (2012) *ACS Catal* 2(9):2022–2028
49. Choudhary V, Caratzoulas S, Vlachos DG (2012) *Carbohydr Res* 368C(10):89–95
50. Danon B, Marcotullio G, Jong WD (2014) *ChemInform* 45(10):39–54